KDM5A Inhibits Antitumor Immune Responses Through Downregulation of the Antigen-Presentation Pathway in Ovarian Cancer

Heng Liu[1], Jianhuang Lin[1], Wei Zhou[1], Renyta Moses[2], Zhongping Dai[1], Andrew V. Kossenkov[3], Ronny Drapkin[4], Benjamin G. Bitler[5], Sergey Karakashev[1], and Rugang Zhang[1]

ABSTRACT

The extent to which effector $CD8^+$ T cells infiltrate into tumors is one of the major predictors of clinical outcome for patients with epithelial ovarian cancer (EOC). Immune cell infiltration into EOC is a complex process that could be affected by the epigenetic makeup of the tumor. Here, we have demonstrated that a lysine 4 histone H3 (H3K4) demethylase, (lysine-specific demethylase 5A; KDM5A) impairs EOC infiltration by immune cells and inhibits antitumor immune responses. Mechanistically, we found that KDM5A silenced genes involved in the antigen processing and presentation pathway. KDM5A inhibition restored the expression of genes involved in the antigen-presentation pathway *in vitro* and promoted antitumor immune responses mediated by $CD8^+$ T cells *in vivo* in a syngeneic EOC mouse model. A negative correlation between expression of *KDM5A* and genes involved in the antigen processing and presentation pathway such as *HLA-A and HLA-B* was observed in the majority of cancer types. In summary, our results establish KDM5A as a regulator of $CD8^+$ T-cell infiltration of tumors and demonstrate that KDM5A inhibition may provide a novel therapeutic strategy to boost antitumor immune responses.

Introduction

Immune cell infiltration is a major predictor of prognosis for many types of cancer, including epithelial ovarian cancer (EOC; refs. 1–3). Multiple studies have demonstrated that tumor genetic or epigenetic makeup may play a role in regulating intratumor immune infiltration and immune evasion (4–7). Given the reversible nature of epigenetic regulation, it is imperative to understand the epigenetic basis of immune infiltration. Such knowledge could be leveraged to develop novel therapeutic approaches that promote immune infiltration to boost antitumor immunity.

Tumor antigen processing and presentation is one of the key elements that is required for antitumor immune responses (8). Expression of the genes involved in the antigen processing and presentation pathway is often altered during tumor development and progression (9). MHC class I plays a key role in the antitumor immune response by binding tumor intracellular peptides (10). Recognition of antigens presented in the context of MHC class I by professional antigen-presenting cells results in activation or priming of $CD8^+$ T-cell response (11). MHC class I is not essential for cancer cell viability and, therefore, cancer cells often reduce expression of genes encoding MHC class I and other genes encoding components of the antigen-presentation machinery to evade immune surveillance (12–14). However, the mechanisms by which cancer cells inhibit antigen processing and presentation to evade immune surveillance are poorly understood. Therefore, it is critically important to study the role of epigenetic regulators of antigen-presentation pathway.

Lysine-specific demethylase 5A (KDM5A), also known as Jumonji/ARID domain-containing protein 1A (JARID1A) or retinoblastoma-binding protein 2 (RBP2), is an oncogene that is often amplified or overexpressed in several types of cancer (15, 16). KDM5A is a demethylase that removes the trimethylation on lysine 4 of histone H3 (H3K4me3) epigenetic mark (17). H3K4me3 mark is present at the promoter sites of transcriptionally active genes (18, 19). By removing H3K4me3, KDM5A represses multiple tumor suppressor genes involved in cell cycle (20), invasion (21), epithelial–mesenchymal transition (EMT; 22), chemoresistance (16, 23), and other processes beneficial for tumor progression (15). Several small-molecule KDM5A inhibitors have been developed and shown to be effective in inhibiting KDM5A enzymatic activity, as evidenced by upregulation of H3K4me3 levels (24–26). Despite the pharmacologic efficacy in blocking KDM5A enzymatic activity, KDM5A inhibitors only demonstrated limited effectiveness at suppressing cancer cell viability as single agents *in vitro* (27). In addition, there is evidence to suggest that KDM5A may exhibit its oncogenic activity through remodeling the tumor immune microenvironment (15). However, the role of KDM5A in controlling antigen-presentation and the associated infiltration of $CD8^+$ T cells remains unclear.

Here we have demonstrated that KDM5A represses expression of genes involved in tumor antigen processing and presentation. This resulted in decreased tumor infiltration by $CD8^+$ T cells and ultimately

[1]Immunology, Microenvironment and Metastasis Program, The Wistar Institute, Philadelphia, Pennsylvania. [2]Cell and Molecular Biology Graduate Group, Biomedical Graduate Studies, Perelman School of Medicine, University of Pennsylvania, Philadelphia, Pennsylvania. [3]Gene Expression and Regulation Program, The Wistar Institute, Philadelphia, Pennsylvania. [4]Department of Obstetrics and Gynecology, Perelman School of Medicine, University of Pennsylvania, Philadelphia, Pennsylvania. [5]Division of Reproductive Sciences, Department of Obstetrics and Gynecology, School of Medicine, The University of Colorado Anschutz Medical Campus, Aurora, Colorado.

Note: Supplementary data for this article are available at Cancer Immunology Research Online (http://cancerimmunolres.aacrjournals.org/).

Current address for Z. Dai: Fox Chase Cancer Center, Philadelphia, Pennsylvania; and current address for S. Karakashev: Fels Cancer Institute for Personalized Medicine, Temple University Lewis Katz School of Medicine, Philadelphia, Pennsylvania.

Corresponding Authors: Rugang Zhang, Immunology, Microenvironment and Metastasis Program, The Wistar Institute 3601 Spruce Street, Philadelphia, PA 19104. Phone: 215-495-6840; E-mail: rzhang@wistar.org; and Sergey Karakashev, sergey.karakashev@temple.edu

Cancer Immunol Res 2022;10:1028–38

doi: 10.1158/2326-6066.CIR-22-0088

inhibited the antitumor immune response. KDM5A inhibition genetically or using small molecule inhibitors restored expression of antigen-presentation genes. Consistent with these data, KDM5A inhibition reduced tumor burden and improved survival of tumor-bearing mice in a $CD8^+$ T-cell–dependent manner in a syngeneic EOC mouse model. Thus, our studies establish KDM5A as an epigenetic therapeutic target whose inhibition boosts the antitumor immune response.

Materials and Methods

Cell culture, transfection, and reagents

ID8 (RRID: CVCL_VA22) cells expressing luciferase were provided by K. Roby (Department of Anatomy and Cell Biology, University of Kansas, Lawrence, KS), and HEK293FT (RRID: CVCL_0045) cells were purchased from ATCC in 2008. These cells were cultured in DMEM (Corning, catalog no. 10–013-CM) supplemented with 10% FBS (R&D Systems, catalog no. S11510) and 1% penicillin/streptomycin (Corning, catalog no. 30–002-CI) at 37°C with 5% CO_2. HGS2 cells (RRID: CVCL_B5GW; gift from Dr. Ronny Drapkin, University of Pennsylvania, Philadelphia, PA) were cultured in DMEM-F12 (Corning, catalog no. 10–092-CM) supplemented with 5% FBS, Insulin/Transferrin/Selenium (Invitrogen, catalog no. 51300), 0.5 mg/mL Hydrocortisone (Sigma, catalog no. H0135), 10 ng/mL murine epidermal growth factor (Sigma, catalog no. E4127) and 1% penicillin/streptomycin at 37°C with 5% CO_2. The human high-grade serous ovarian cancer (HGSOC) cell lines A1847 (RRID:CVCL_9724), PEO4 (RRID:CVCL_2690), OVSAHO (RRID:CVCL_3114), OVCAR10 (RRID:CVCL_4377), OVCAR3 (RRID:CVCL_0465), CAOV3 (RRID:CVCL_0201), COV382 (RRID:CVCL_2420), Kuramochi (RRID:CVCL_1345) were cultured in RPMI1640 (Corning, catalog no. 10–040-CM) supplemented with 10% FBS and 1% penicillin/streptomycin at 37°C with 5% CO_2. The human fallopian tube epithelial cells FT246 (RRID:CVCL_UH61) and FT237 (RRID: CVCL_UH59) were gifts from R. Drapkin at the University of Pennsylvania, and they were grown in DMEM-F12 with 10% FBS. All cell lines were authenticated at The Wistar Institute (Philadelphia, PA) Genomics Facility using short tandem repeat DNA profiling. *Mycoplasma* testing was performed using LookOut *Mycoplasma* PCR detection (Sigma, catalog no. MP0035) every month. Cells were cultured for a maximum of 2 months or 20 passages.

Colony formation

Cells were seeded in 24-well plates with different numbers according to growth rate. RPMI medium with 10% FBS and 1% penicillin/streptomycin was used for all colony-formation experiments. Medium was changed every 2 days with appropriate drug doses for 10 to 12 days. Colonies were stained with 0.05% crystal violet (Sigma, catalog no. 6158). The signal was quantified by intensity using NIH ImageJ software.

Antibodies

For Western blotting, the following primary antibodies were used: mouse anti–β-actin (Sigma, catalog no. A5316), rabbit anti-KDM5A (Abcam, catalog no. ab194286, RRID: AB_1139986; Cell Signaling Technology, catalog no. 3876S, RRID: AB_2129055), mouse anti-H3K4me3 (Abcam, catalog no. ab12209, RRID: AB_442957), anti-mouse IgG horseradish peroxidase (HRP; Cell Signaling Technology, catalog no. 7076, RRID: AB_330924), and anti-rabbit IgG HRP (Cell Signaling Technology, catalog no. 7074, RRID: AB_2099233). For IHC, rabbit anti-KDM5A (Cell Signaling Technology, catalog no. 3876S, RRID: AB_ 2129055) was used. For *in vivo* mouse experiments, anti-mouse CD8 (BioXcell, catalog no. BE0061, RRID: AB_10950145) and rat IgG2b isotype control (BioXcell, catalog no. BE0090, RRID: AB_1107780) were used.

CRISPR-mediated knockouts

pLentiCRISPR v2 (Addgene, catalog no. 52961, RRID: Addgene_52961) was digested with BsmBI (New England Biolabs, catalog no. R0580) at 55°C for 1 hour and run on a 1% agarose gel. The digested plasmid was cut out and purified using QIAquick gel extraction kit (Qiagen, catalog no. 166047244). Oligonucleotide pairs were phosphorylated using T4 PNK (New England Biolabs, catalog no. M0201S) in T4 ligation buffer (New England Biolabs) and annealed in a thermocycler at 37°C for 30 minutes, 95°C for 5 minutes, ramped down to 25°C at 5°C per minute. Annealed oligonucleotide pairs were diluted 1:200 in RNase/DNase-free water. Ligation of the annealed oligonucleotide and digested pLentiCRISPR v2 plasmid was performed using Quick Ligase (New England Biolabs, catalog no. M2200L). The following oligonucleotides were used for cloning: mouse *Kdm5a gRNA#1(*5′- AGTGTGTAAATCACTATCGA-3) or mouse *Kdm5a gRNA#2* (5′- ATGCGCCCGATAAAACTCAG-3).

Tet-inducible knockdown of *Kdm5a* using short hairpin RNA

tet-pLKO-shKdm5a was constructed by inserting the sense sequence 5′- CCTTTGAGTGACTTAGAGGAA-3′ for clone 1 or 5′- CAAAGAGAACAAGACGAGTTA-3′ for clone 2 into the tet-pLKO-puro vector (Addgene, catalog no. 21915) digested with AgeI (New England Biolabs, catalog no. R3552) and EcoRI restriction enzymes (New England Biolabs, catalog no. R3010) and dephosphorylated for 30 minutes at 37°C. The digested plasmid was run on a 1% agarose gel, cut out, and purified using the Wizard SV Gel and PCR Clean Up kit (Promega, catalog no. A9281). The oligonucleotides were phosphorylated using T4 PNK (New England Biolabs, catalog no. M0201S) with T4 Ligation Buffer (New England Biolabs, catalog no. B0202S). Samples were annealed in a thermocycler at 37°C for 30 minutes and then at 95°C for 5 minutes and finally were ramped down to 25°C at 5°C per minute. Annealed oligonucleotides were diluted 1:200 in RNase/DNase-free water. Ligation of the annealed oligonucleotide and digested tet-pLKO-puro plasmid was performed using Quick Ligase (New England Biolabs, catalog no. M2200S). To induce *Kdm5a* knockdown, cells infected with tet-inducible short hairpin (sh)Kdm5a virus were treated with 2 μg/mL of doxycycline (Sigma, catalog no. 324385).

Lentivirus infection

HEK293FT cells were transfected with target vector, psPAX2 (Addgene, catalog no. 12260, RRID: Addgene_12260) and pCMV-VSV (Addgene, catalog no. 8454, RRID: Addgene_8454) by Lipofectamine 2000 (Life Technologies, catalog no. 11668027) for 6 hours and replaced with fresh medium, as per the manufacturer's instructions. Lentivirus was harvested and filtered with a 0.45-μm filter 72 hours posttransfection. Cells were infected by culturing them in half filtered virus-containing medium and half fresh medium for 48 hours and selected in medium containing 1 μg/mL puromycin (Gibco, catalog no. A1113803).

IFNγ, CPI-455, and doxycycline treatment *in vitro*

For IFNγ-induced MHC class I antigen expression, ID8 and HGS2 cells were treated with or without 20 ng/mL IFNγ (Stem Cell Technologies, catalog no. 78021.1) for 24 hours. For the KDM5A inhibitor CPI-455, cells were treated with or without 10 μmol/L CPI-455 (Medkoo, catalog no. 406987) for 8 days with fresh drug-

containing media added every 3 days. To induce *Kdm5a* knockdown, cells expressing tet-inducible shKdm5a were treated with 2 μg/mL of doxycycline (Sigma, catalog no. 324385) for at least one week with fresh drug-containing media every 3 days.

Immunoblots

Cells were trypsinized and washed two times with PBS. Protein was extracted with RIPA lysis buffer [50 mmol/L Tris (pH 8.0), 150 mmol/L NaCl, 1% Triton X-100, 0.5% sodium deoxycholate, 0.1% SDS, and 1 mmol/L phenylmethylsulfonyl fluoride (PMSF)] on ice for 30 minutes. Protein concentration was measured by the bicinchoninic acid (BCA) assay (Pierce, catalog no. 23225). Samples were separated by SDS-PAGE and transferred to polyvinylidene fluoride membrane (Millipore, catalog no. IPVH00010). Membranes were blocked with 4% BSA/TBS-T and then incubated with primary antibodies and secondary antibodies (see Antibodies). Antibody binding was visualized using enhanced chemiluminescence (ECL; Thermo Fisher Scientific, catalog no. 32209).

qRT-PCR

Total RNA was extracted using RNeasy Kit (Qiagen, catalog no. 74106) following the manufacturer's instructions. One microgram purified RNA was used for RT-PCR with High-Capacity cDNA Reverse Transcription Kit (Thermo Fisher Scientific, catalog no. 4374967). qPCR was performed using iTaq Universal SYBR Green Supermix (Bio-Rad, catalog no. 1725121) and run on QuantStudio 5 Real-Time PCR System with three biological repeats. Change in expression was calculated based on the $2^{-\Delta\Delta CT}$. The primer sequences used were as follows: mouse *β-actin*, forward: 5′-CTCCTATGTGGGTGACGAGG-3′ and reverse: 5′-ACGGTTGGCCTTAGGGTTC-3′, mouse *H2K1*, forward: 5′-ACCAGCAGTACGCCTACGA-3′ and reverse: 5′-AACCAGAACAGCAACGGTCG-3′.

Chromatin immunoprecipitation followed by qPCR

Chromatin immunoprecipitation (ChIP) was performed as previously described (28). The following antibodies were used for ChIP: rabbit anti-KDM5A (Abcam, catalog no. ab194286, RRID: AB_1139986, 5 μg per IP) and mouse anti-H3K4me3(Abcam, catalog no. ab12209, RRID: AB_442957, 2 μg per IP). Isotype-matched IgGs were used as negative controls. DNA for ChIP was purified using the Zymo ChIP DNA clean and concentrator kit (Zymo Research, catalog no. D5205) and analyzed by qPCR. The following primers were used for qPCR: *H2K1*, forward: 5′-CTGCCTGGCGACTAAGACTT-3′ and reverse: 5′-ACTCCAGGGTCTGACTTCTGA-3′.

Flow cytometry analysis

For cell surface MHC class I H2-K1 expression analysis, ID8 or HGS2 cells were treated by 10 mmol/L EDTA [in Dulbecco's Phosphate-Buffered Saline (DPBS)] and washed twice with DPBS. Cells were then blocked by Fc blocking buffer (BD Biosceinces, catalog no. 553142, RRID: AB_394657) on ice for 30 minutes and then stained with PE-conjugated anti–MHC-1 (Abcam, catalog no. ab25547, RRID: AB_470631) for another 30 minutes. After washing with DPBS twice, MHC-1 staining was detected using a Becton–Dickinson LSR18/LSR14 machine, and analyzed with FlowJo version 10 software (Tree Star, Inc.)

For immune infiltration analysis, cells from ascites were collected, after lysis of red blood cells with RBC buffer (BioLegend, catalog no. 420302). The cells were sequentially filtered through a 40-μm cell strainer. Analysis of tumor-infiltrating lymphocytes (TIL) involved viability staining (Thermo Fisher Scientific, catalog no. L34957), Fc blocking (BD Biosciences, catalog no. 553142, RRID:AB_394657) and then surface staining in FACS buffer (3% FBS in PBS) with fluorochrome-conjugated antibodies against mouse CD45 (BioLegend, catalog no. 103147, RRID:AB_2564383), mouse CD3 (BD Biosciences, catalog no. 552774, RRID:AB_394460), mouse CD4 (BioLegend, catalog no. 100516, RRID:AB_312719), mouse CD8 (BioLegend, catalog no. 100708, RRID:AB_312747), mouse CD19 (BioLegend, catalog no. 115523, RRID:AB_439718), mouse CD69 (BioLegend, catalog no. 104510, RRID:AB_313113), mouse PD-L1 (BioLegend, catalog no. 124321, RRID:AB_2563635), mouse PD-1 (BioLegend, catalog no. 135214, RRID:AB_10680238), mouse CD11c (BioLegend, catalog no. 117324, RRID:AB_830649), and mouse CD11b (BioLegend, catalog no. 101259, RRID:AB_2566568). All flow cytometry analyses were performed on a BD LSR II or a Canto II Flow Cytometer, and data were analyzed with FlowJo software (Tree Star, Inc., version 10).

IHC

HGSOC tumor tissue microarrays (TMA) were kindly provided by Dr. Benjamin G. Bitler from The University of Colorado (Boulder, CO; COMIRB# 17–7788). Detailed information on the tumors contained on the TMA has been published previously (29, 30). IHC was performed using Dako EnVision+ system (Dako, catalog no. K4002) following the manufacturer's instructions. Briefly, antigen retrieval was performed by boiling in sodium citrate buffer (Thermo Fisher Scientific, catalog no. 005000) for 45 minutes. The sections were deparaffinized, rehydrated, and immersed in 3% hydrogen peroxide in methanol to quench endogenous peroxidase activity. The sections were incubated with blocking buffer for 1 hour, primary antibody against KDM5A (Cell Signaling Technology, catalog no. 3876S, RRID: AB_ 2129055) at 4°C overnight and secondary antibody for 1 hour. After washing, tissue sections were incubated with DAB (Dako, catalog no. GV82511–2) to visualize the staining signal. Counterstaining was performed using Mayer's Hematoxylin (Dako, catalog no. 3309S). Images were captured using a Nikon ECLIPSE Ni-U microscope.

Syngeneic ovarian cancer mouse model

All animal protocols described in this study were approved by the Institutional Animal Care and Use Committee (IACUC) at The Wistar Institute. 6- to 8-week-old female wild-type C57BL/6 mice were purchased from Charles River Laboratories and the age-matched female NOD/SCID gamma (NSG) mice were bred at The Wistar Institute Animal Facility. Briefly, 2×10^6 of 70% confluent doxycycline-inducible shKdm5a ID8 cells were injected into the peritoneal cavity of mice and allowed to establish tumors. After 1 week, mice were randomized into two groups and treated with control (Bio-Serv, catalog no. S4207) or doxycycline-containing diet (Bio-Serv, catalog no. S3888) for 4 weeks. Tumor growth was followed by noninvasive imaging using an IVIS Spectrum 15 to 20 minutes after mice were administered D-Luciferin potassium salt (150 mg luciferin/kg body weight; Perkin Elmer, catalog no. 122799). Images were analyzed using Live Imaging 4.0 software. After 4 weeks of treatment ascites volume was measured as an additional surrogate for tumor burden. For anti-CD8 treatment, 2×10^6 of 70% confluent doxycycline-inducible shKdm5a ID8 cells were injected into the peritoneal cavity of mice and allowed to establish tumors. After 1 week, mice were randomized into four groups and treated with control (Bio-Serv, catalog no. S4207) or doxycycline containing diet (Bio-Serv, catalog no. S3888) in the presence of an anti-CD8 (BioXcell, catalog no. BE0061, RRID: AB_10950145) or a rat IgG2b isotype control (BioXcell, catalog no.

BE0090, RRID: AB_1107780), 500 μg per mouse, twice a week. For CPI-455 treatment, 2×10^6 of 70% confluent ID8 cells were injected into the peritoneal cavity of mice and allowed to establish tumors. After 1 week, mice were randomized into two groups and treated with vehicle control or CPI-455 (Medkoo, catalog no. 406987) 50 mg/kg, twice a week. After 4 weeks of treatment ascites volume was measured as a surrogate for tumor burden. Timelines for all *in vivo* experiments are described in Supplementary Table S1.

CIBERSORT

CIBERSORT was used for the estimation of immune cell infiltration using transcriptome data from the 300 samples in The Cancer Genome Atlas (TCGA) HGSOC dataset (31). Gene expression profiles of the 300 cases were uploaded to CIBERSORT as a mixture file (31), and CIBERSORT was run with absolute mode option using LM22 signature gene file, 1,000 permutations, and quantile normalization disabled. Pearson correlation was used to test association between $CD8^+$ T-cell signature score and every gene expression in 300 TCGA HGSOC samples.

RNA sequencing

Total RNA of control ID8 and *Kdm5a*-knockout (KO) ID8 cell lines was extracted using the RNeasy mini Kit (Qiagen, catalog no. 74106) and digested with DNase I (Qiagen, catalog no. 79254). RNA sequencing (RNA-seq) libraries were constructed using ScriptSeq complete Gold kit (Epicentre, catalog no. SCL24EP) and subjected to a 75-bp paired-end sequencing run on NextSeq 500, using Illumina's NextSeq 500 high output sequencing kit following the manufacturer's instructions.

CUT&RUN sequencing

For CUT&RUN sequencing, cells were harvested by trypsinization and gently washed twice using wash buffer [20 mmol/L HEPES pH 7.5, 150 mmol/L NaCl, 0.5 mmol/L spermidine, and EDTA-free Protease Inhibitor Cocktail (Sigma, catalog no. 11873580001)]. Cells were then incubated with the anti-KDM5A (Cell Signaling Technology, catalog no. 3876S, RRID:AB_2129055) at 4 °C overnight in antibody buffer (wash buffer supplemented with 0.05% digitonin and 2 mmol/L EDTA). The next day, supernatant was removed by centrifugation and cell pellets were washed once with Dig-wash buffer (Wash buffer containing 0.05% digitonin). Cell pellets were then incubated with Protein A/G MNase (Cell Signaling Technology, catalog no. 40366; 700 ng/mL in Dig-wash buffer) for 1 hour by rotation at 4 °C. After three times of washes, cell pellets were resuspended in 100 μL Dig-wash buffer with 2 μL 100 mmol/L $CaCl_2$ and incubated at 0 °C for 30 minutes; reactions were stopped by addition of 100 μL 2× STOP buffer (340 mmol/L NaCl, 20 mmol/L EDTA pH 8.0, 4 mmol/L EGTA, 0.05% digitonin, 50 μg/ml RNase A, 50 μg/ml glycogen). The supernatant DNA was collected after centrifugation and further purified using phenol–chloroform–isoamyl alcohol (Sigma, catalog no. p3803) extraction and ethanol precipitation. Purified DNA was used for library construction using the NEBNext Ultra DNA Library Prep Kit (New England Biolabs, catalog no. E7645) following the manufacturer's instructions, and the libraries were sequenced in a 75-base pair single-end run on the Next Seq 500 (Illumina) at Wistar Genomic facility.

Bioinformatics and statistical analysis

RNA-seq data was aligned using bowtie2 (32) against 10-mm version of the mouse genome and RSEM v1.2.12 software was used to estimate raw read counts and fragments per kilobase of transcript per million mapped reads values using Ensemble transcriptome information. DESeq2 (33) was used to estimate significance of differential expression between Kdm5a-KO and parental samples. Overall gene expression changes were considered significant if FDR < 5%. CUT&RUN data was aligned using bowtie (34) against 10-mm version of the mouse genome and HOMER (35) was used to call significant peaks in using "-histone" option. Genes that had a significant H3K4Me3 peak and Kdm5a binding signal of at least 4-fold over control within 500 bp from transcription starting site (TSS) were considered and overlapped with genes significantly upregulated in Kdm5a-KO cells. Significance of overlap was tested using hypergeometric test using 21,588 expressed Ensemble genes as a population size. Gene set enrichment analysis (GSEA) of gene sets was done using GSEA Pathway Analysis (36) using "KEGG pathway database". TCGA Agilent RNA-seq expression data for 300 HGSOC samples with copy number variation calls was downloaded from cBioPortal (37). Expression of *CD8A*, *GZMB*, *HLA-A*, and *HLA-B* was tested for negative association with *KDM5A* expression. *KDM5A* expression data was tested for differences between samples with amplified *KDM5A* versus nonamplified *KDM5A* using two sample Student *t* test. Statistical analyses were performed using GraphPad Prism 6 (GraphPad). Quantitative data are expressed as mean ± SEM unless otherwise stated. Pearson test was used to measure statistical correlation. Kaplan–Meier analysis was used for assessing the overall survival (OS). For all statistical analyses, the level of significance was set at 0.05.

Data mining

For expression correlation analysis, TCGA HGSOC RNA-seq data (PanCancer Atlas, $n = 300$) was downloaded from cBioPortal (https://www.cbioportal.org/) and Cancer Cell Line Encyclopedia (CCLE, $n = 912$). RNA-seq data were downloaded from (https://sites.broadinstitute.org/ccle/datasets). Pearson correlation was used for calculating *P* and *r* values in Microsoft Excel. Pearson correlations between *KDM5A* and *CD8A*, *GZMB*, *HLA-A*, and *HLA-B* were analyzed in 24 of 33 types of TCGA PanCancer Atlas datasets with more than 100 cases. The analysis was performed on the cBioPortal website.

Data availability

Published microarray datasets that include gene expression profiles for HGSOC tissues ($n = 53$) and normal ovarian surface epithelial tissues ($n = 10$) (38), or HGSOC tissues ($n = 13$) and fallopian tube epithelial tissues ($n = 24$; ref. (39) from laser capture microdissections were downloaded from the Gene Expression Omnibus (GEO). mRNA expression levels were compared using GraphPad Prism 7 software. The RNA-seq and CUT&RUN data was submitted to the GEO database and can be accessed using accession number GSE194361. All other data supporting the findings of this study are available within the article and its supplementary data files or are available upon request.

Results

KDM5A expression negatively correlates with the infiltration of $CD8^+$ T cells

To identify epigenetic regulators of $CD8^+$ T-cell infiltration of HGSOC in a systematic and unbiased way, we analyzed the TCGA HGSOC dataset to find epigenetic regulators whose expression was negatively correlated with the $CD8^+$ T-cell signature score using CIBERSORT (**Fig. 1A**; Supplementary Table S2). To focus on those epigenetic regulators with potential for therapeutic targeting, we assessed whether there was a negative association between high

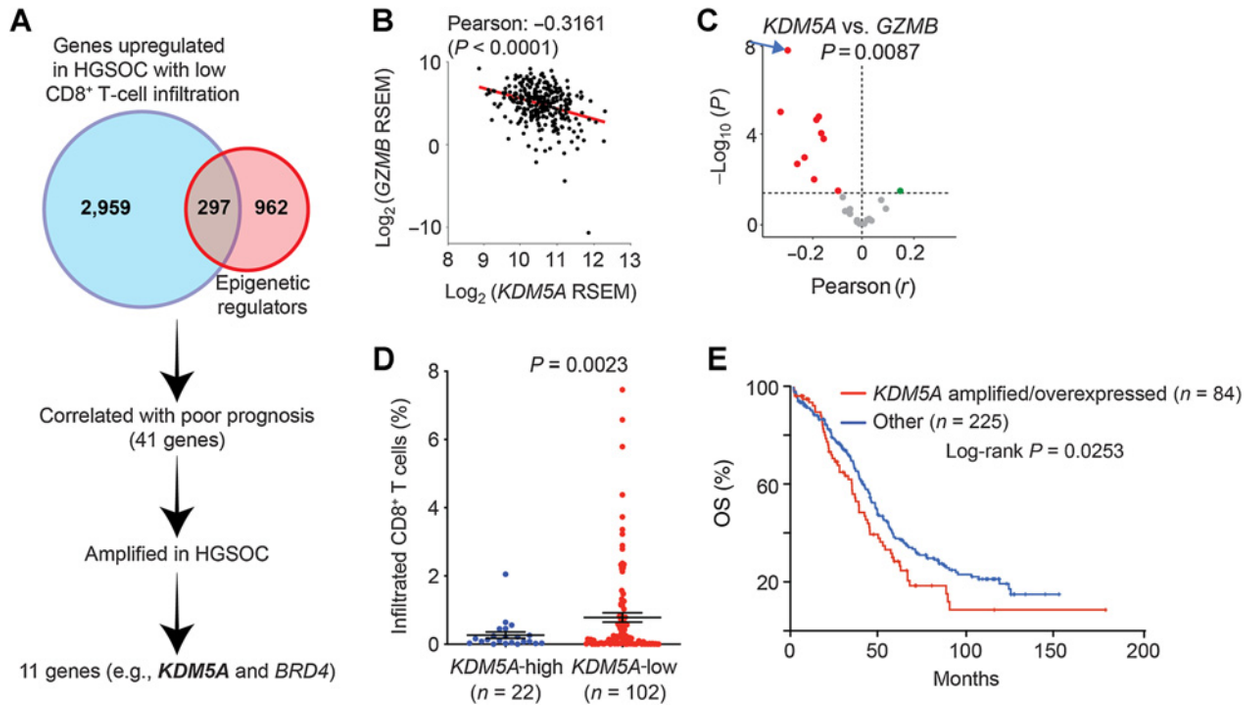

Figure 1.

KDM5A is amplified in EOC and its amplification/overexpression negatively correlates with infiltration of CD8$^+$ T cells. **A,** Schematic of the experimental design for the identification of epigenetic factors regulating infiltration of CD8$^+$ T cells in the TCGA HGSOC dataset. **B,** Correlation between *KDM5A* and *GZMB* expression based on RNA-seq analysis in the TCGA HGSOC dataset. **C,** Significant correlation between *KDM5A* and *GZMB* expression based on RNA-seq analysis from 24 TCGA cancer types with at least 100 patients. The arrow indicates HGSOC. **D,** High *KDM5A* expression correlates with significantly lower levels of CD8$^+$ T-cell infiltration in 124 cases of HGSOC. **E,** Comparison of OS between HGSOC with or without *KDM5A* amplification/overexpression in the TCGA HGSOC dataset. Data represent mean ± SEM; *P* values were calculated by using a two-tailed Student *t* test except in (**B**) by using Pearson *r* analysis, in (**C**) by using Fisher exact test, and in (**E**) using log–rank test.

expression of the epigenetic regulators and OS. 11 genes met those criteria (Supplementary Table S2). Validating our approach, our analysis identified several genes that have been previously implicated in regulation of immune infiltration such as *BRD4*, *CHD4*, and *GSK3B* (Supplementary Table S2; refs. 40–42). KDM5A, an H3K4me3 demethylase, was the top epigenetic factor identified by this approach, and it has not been previously associated with the regulation of infiltration of CD8$^+$ T cells (Supplementary Fig. S1A; Supplementary Table S2). We also observed a negative correlation between *KDM5A* and *CD8A* expression among an independent dataset consisting of 53 laser-capture microdissected HGSOCs (Supplementary Fig. S1B). Furthermore, *KDM5A* expression negatively correlated with *GZMB* and *PRF1* expression, activation markers for CD8$^+$ T cells, in the HGSOC TCGA dataset (**Fig. 1B**; Supplementary Fig. S1C). Finally, a negative correlation between expression of *KDM5A* and *GZMB* was observed in a significant number of the cancer types among the 24 TCGA datasets with more than 100 patients (**Fig. 1C**; Supplementary Table S3).

We next sought to assess the correlation between KDM5A protein expression and intratumor CD8$^+$ T-cell infiltration in a tumor microarray consisting of 124 cases of human HGSOCs. We observed that low KDM5A expression was associated with double the amount of intratumor CD8$^+$ T-cell infiltration (**Fig. 1D**; Supplementary Fig S1D). Low levels of CD8$^+$ T-cell infiltration are a major factor associated with poor survival in HGSOCs (43–45). Consistent with this, we observed that high *KDM5A* expression was associated with poor prognosis in the TCGA HGSOC dataset (**Fig. 1E**). In addition, *KDM5A* was upregulated in HGSOCs compared with normal tissues from laser-capture microdissections (Supplementary Fig. S1E). In addition, *KDM5A* expression was found to be upregulated in 75% (6/8) EOC cell lines tested compared with fallopian tube epithelial cells (Supplementary Fig. S1F). We conclude that high KDM5A expression negatively correlates with CD8$^+$ T-cell infiltration and associates with poor survival in HGSOCs.

We next sought to determine whether inhibition of KDM5A activity affected the growth of EOC cells. Toward this goal, we treated a panel of EOC cell lines with various degree of KDM5A expression with CPI-455, a small molecule inhibitor of KDM5A (46). Consistent with previous studies (47), CPI-455 did not significantly affect cell viability *in vitro* regardless of KDM5A expression status in a dose response curve analysis (Supplementary Fig. S1G). Thus, we conclude that KDM5A inhibition does not affect the growth of EOC cells.

KDM5A inhibition promotes antitumor immune responses *in vivo*

Since KDM5A inhibition did not affect the viability of EOC cells, we sought to determine whether KDM5A influenced the EOC tumor immune microenvironment. Toward this goal, we developed a doxycycline-inducible shRNA-mediated *Kdm5a*-knockdown version of the mouse EOC cell line ID8. Induced depletion of Kdm5a led to increased levels of H3K4me3, the substrate of Kdm5a (**Fig. 2A**). Consistent with

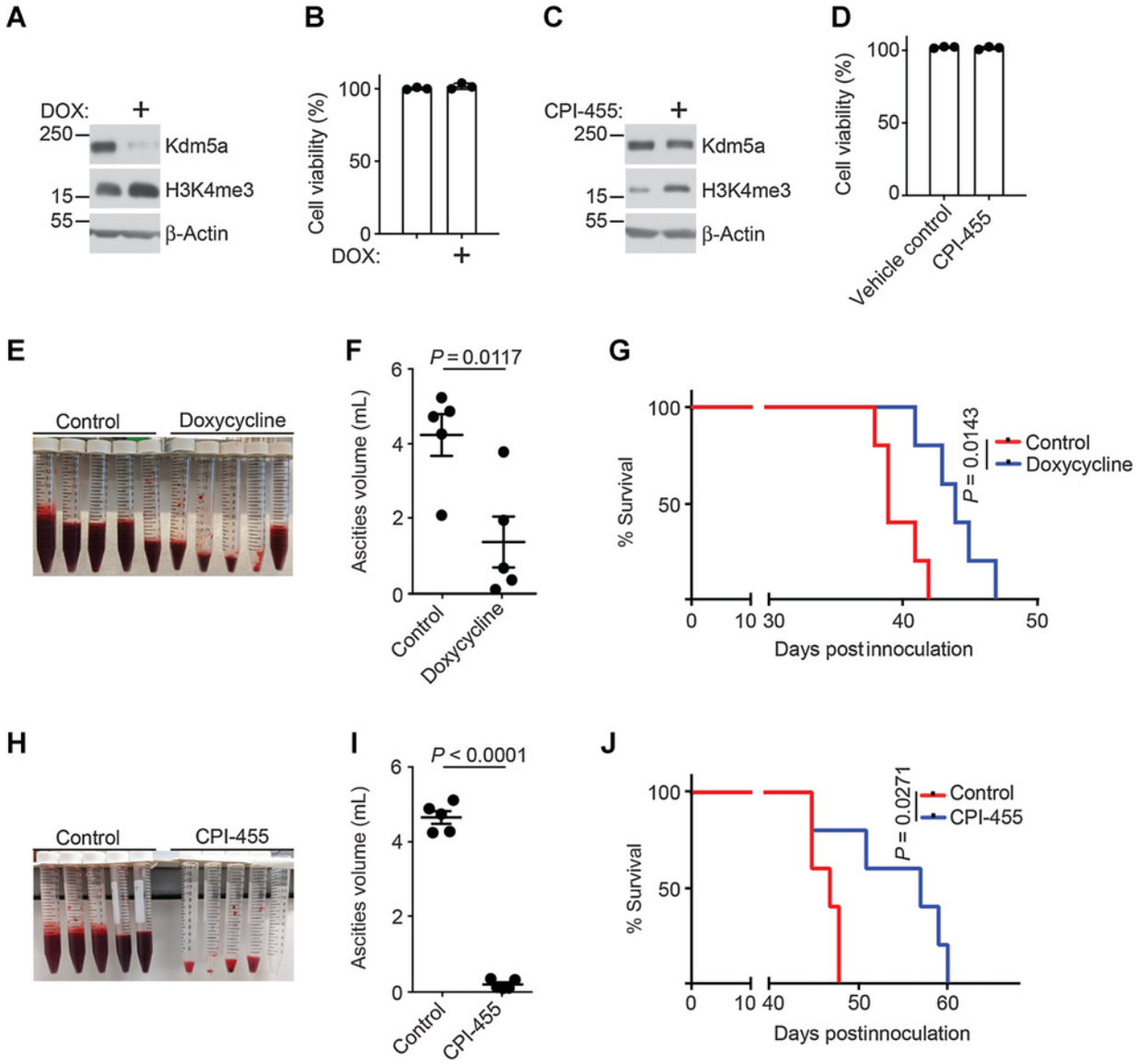

Figure 2.

KDM5A inhibition suppresses tumor growth *in vivo* in an immune-competent mouse model of ovarian cancer. **A,** Expression of Kdm5a, H3K4me3, and a loading control β-actin in doxycycline-inducible shKdm5a ID8 mouse EOC cells treated with or without 2 μg/mL of doxycycline. **B,** ID8 cells were plated into 24-well plates and treated with 2 μg/mL of doxycycline the same day. Cells were incubated for 8 days. Relative cell viability was determined by colony formation assay. **C,** Expression of Kdm5a, H3K4me3, and a loading control β-actin in ID8 cells treated with 10 μmol/L CPI-455 or vehicle control. **D,** ID8 cells were plated into 24-well plates and incubated with 10 μmol/L CPI-455 for 8 days with fresh drug-containing media every 3 days. Relative cell viability was determined by colony formation assay. **E,** Ascites produced in C57BL/6 mice injected with doxycycline-inducible shKdm5a ID8 cells treated with control or doxycycline-containing food. **F,** Quantification of ascites volumes from (**E**). **G,** Kaplan–Meier survival curves for the indicated groups. **H,** Ascites produced in C57BL/6 mice injected with ID8 cells treated with vehicle control or KDM5A inhibitor CPI-455. **I,** Quantification of ascites volumes from (**H**). **J,** Kaplan–Meier survival curves for the indicated groups. Data represent mean ±SEM of three biological repeats or 5 mice per group; *P* was calculated by using a two-tailed Student *t* test except in (**G**) and (**J**) by log–rank tests. DOX, doxycycline.

the observation that KDM5A inhibition failed to affect the viability of human EOC cell lines regardless of KDM5A expression levels, shRNA-mediated *Kdm5a* knockdown did not affect the growth of ID8 cells *in vitro*. (**Fig. 2B**). Similar observations were made in two independent ID8 inducible shKdm5a clones (**Fig. 2A** and **B**; Supplementary Fig. S2A and S2B). Likewise, the small-molecule inhibitor of KDM5A CPI-455 did not affect cell viability, even though it increased H3K4me3 levels in two mouse EOC cell lines ID8 and HGS2 (**Fig. 2C** and **D**; Supplementary S2C and S2D).

To determine the effects of KDM5A inhibition on the growth of KDM5A-expressing EOC *in vivo*, we utilized a syngeneic immuno-competent EOC mouse model. Specifically, immune-competent C57BL/6 mice were injected intraperitonially with luciferase-expressing doxycycline-inducible shKdm5a-expressing mouse EOC

ID8 cells. Cells were allowed to grow for 1 week and then mice were randomized based on luciferase signal. Mice were next treated with or without doxycycline-containing food as previously reported (48). Doxycycline treatment significantly reduced the tumor burden as measured by luminescence, which correlated with improved survival of tumor-bearing mice; this was seen for two independent ID8 doxycycline-inducible shKdm5a clones (**Fig. 2E**-**G**; Supplementary Fig. S2E and S2F). Doxycycline treatment also significantly reduced the amount of ascites produced, a key feature of EOC clinical presentation (**Fig. 2E** and **F**; Supplementary Fig. S2G and S2H; ref. 49). Also, doxycycline treatment did not affect the body weight of tumor bearing mice (Supplementary Fig. S2I). As a control, doxycycline treatment did not significantly inhibit tumor cell growth *in vivo* or affect the survival of tumor-bearing mice established in parallel in immune-compromised NSG mice (Supplementary Fig. S2J and S2K). Together, these data led us to conclude that *Kdm5a* knockdown reduces tumor burden and improves the survival of tumor-bearing mice in an immune-competent but not in an immune-compromised mouse EOC model.

We next sought to complement the *in vivo* genetic knockdown studies using the KDM5A inhibitor CPI-455. Toward this goal, ID8 cells were first injected intraperitonially in immunocompetent C57BL/6 mice and the cells were allowed to grow for 1 week to establish the tumors. Mice were then randomized and treated daily with vehicle control or CPI-455 (50 mg/kg) by i.p. injection. Similar to *Kdm5a* knockdown, CPI-455 treatment significantly reduced ascites production and improved the survival of tumor-bearing mice (**Fig. 2H**–**J**). Thus, we conclude that the antitumor effect of KDM5A inhibition depends on the immune microenvironment.

Antitumor immune responses induced by KDM5A inhibition depend on CD8$^+$ T cells

To test our hypothesis that KDM5A inhibition reduces tumor growth through regulation of immune infiltration, we profiled changes in immune cells in ascites collected from mice bearing doxycycline-inducible shKdm5a ID8 cells in the presence or absence of doxycycline (Supplementary Fig. S3A). Consistent with our CIBERSORT analysis, we observed an increase in the percentage and total number of CD8$^+$ T cells in mice bearing tumors with depleted Kdm5a levels (**Fig. 3A**; Supplementary Fig. S3B). In addition to an increased total number of CD8$^+$ T cells, we also observed that Kdm5a inhibition resulted in an increase in the percentage of activated CD8$^+$ T cells, as assessed by CD69 expression (**Fig. 3B**). Previous studies have demonstrated that KDM5A potentially regulates immune responses by altering immune checkpoint pathways (50). Accordingly, we tested PD-L1 expression on the surface of tumor cells and CD11b$^+$ myeloid cells as well as PD-1 expression on the surface of CD4$^+$ T and CD8$^+$ T cells isolated from ascites. We observed that Kdm5a depletion led to a decrease in in the percentage of CD8$^+$ T cells expressing PD-1$^+$ (Supplementary Fig. S3C). However, we did not observe any significant effect of Kdm5a depletion on PD-L1 expression in either cancer or myeloid cells (Supplementary Fig. S3D). Likewise, we observed no changes in PD-1 expression on CD4$^+$ T cells (Supplementary Fig. S3D). In contrast to CD8$^+$ T cells, the percentage of other immune cell types, including dendritic cells, myeloid cells, and B cells, did not increase in ascites collected from mice bearing Kdm5a-depleted ID8 cells (Supplementary Fig. S3E). Infiltration of cytotoxic CD8$^+$ T cells plays a critical role in promoting antitumor immune responses. Thus, we next sought to investigate whether the antitumor effects promoted by Kdm5a inhibition depended on CD8$^+$ T cells. Toward this goal, we used an anti-CD8 to deplete CD8$^+$ T cells in immune-competent

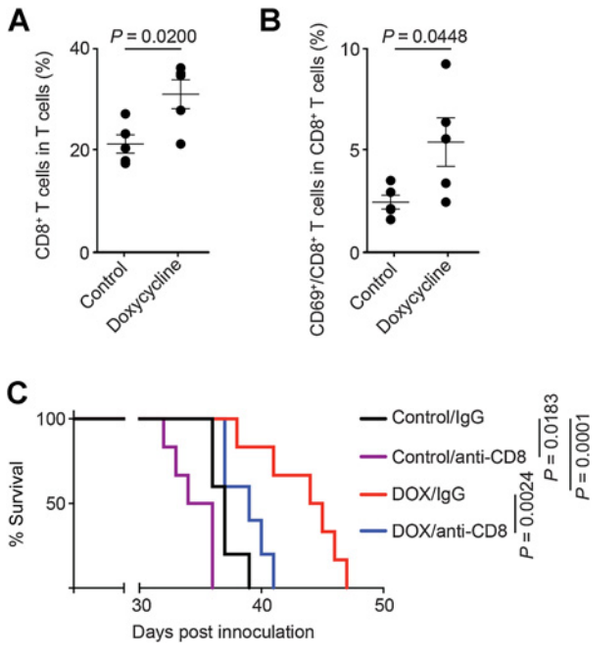

Figure 3.

CD8$^+$ T cells mediate antitumor immune responses induced by KDM5A inhibition. Mice bearing tumors formed by ID8 cells expressing doxycycline-inducible shKdm5a were fed a doxycycline-containing diet to induce *Kdm5a* knockdown. Infiltration of CD8$^+$ T cells (**A**) or activated CD69$^+$CD8$^+$ T cells **(B)** in ascites collected from the indicated treatment groups were analyzed by flow cytometry at the end of experiment ($n = 5$ mice per group). Data represent mean ±SEM; *P* values were calculated using a two-tailed *t* test. Kaplan–Meier survival curves for the indicated groups ($n = 5$ mice per group; **C**). *P* was calculated by log-rank test. DOX, doxycycline.

C57BL/6 mice bearing doxycycline-inducible shKdm5a ID8 cells in the presence or absence of doxycycline. We observed that anti-CD8 treatment abrogated the antitumor effect of Kdm5a inhibition *in vivo*, as evidenced by the loss of improvement of survival of tumor-bearing mice (**Fig. 3C**). Thus, our data demonstrate that CD8$^+$ T cells mediate the antitumor immune effects induced by KDM5A inhibition.

KDM5A regulates antigen processing and presentation pathway

To explore the mechanistic basis of Kdm5a-regulated tumor infiltration by CD8$^+$ T cells, we performed RNA-seq in parental control and Kdm5a-KO ID8 cells. Since KDM5A functions as a suppressor of gene expression (17), we focused our analysis on genes that were upregulated by *Kdm5a* KO. This analysis revealed a list of 2,966 genes that were significantly differentially expressed (FDR < 5%) by *Kdm5a* KO in ID8 cells compared with control cells (**Fig. 4A**; Supplementary Fig. S4A). To identify direct Kdm5a target genes, we performed CUT&RUN for Kdm5a and its enzymatic substrate H3K4me3 in control and *Kdm5a*-KO ID8 cells (**Fig. 4A**). This analysis revealed a list of 13,569 genes that were occupied by Kdm5a/H3K4me3. Cross-referencing RNA-seq and CUT&RUN data revealed a list of 2,496 direct Kdm5a target genes that were differentially expressed in *Kdm5a*-KO ID8 cells (**Fig. 4A**). This represents a significant overlap (1.6-fold over expected by chance, $P = 4.4 \times 10^{-323}$) between 2,966 genes that were differentially expressed in Kdm5a-KO cells compared with control ID8 cells and 13,569 genes that were occupied by Kdm5a/

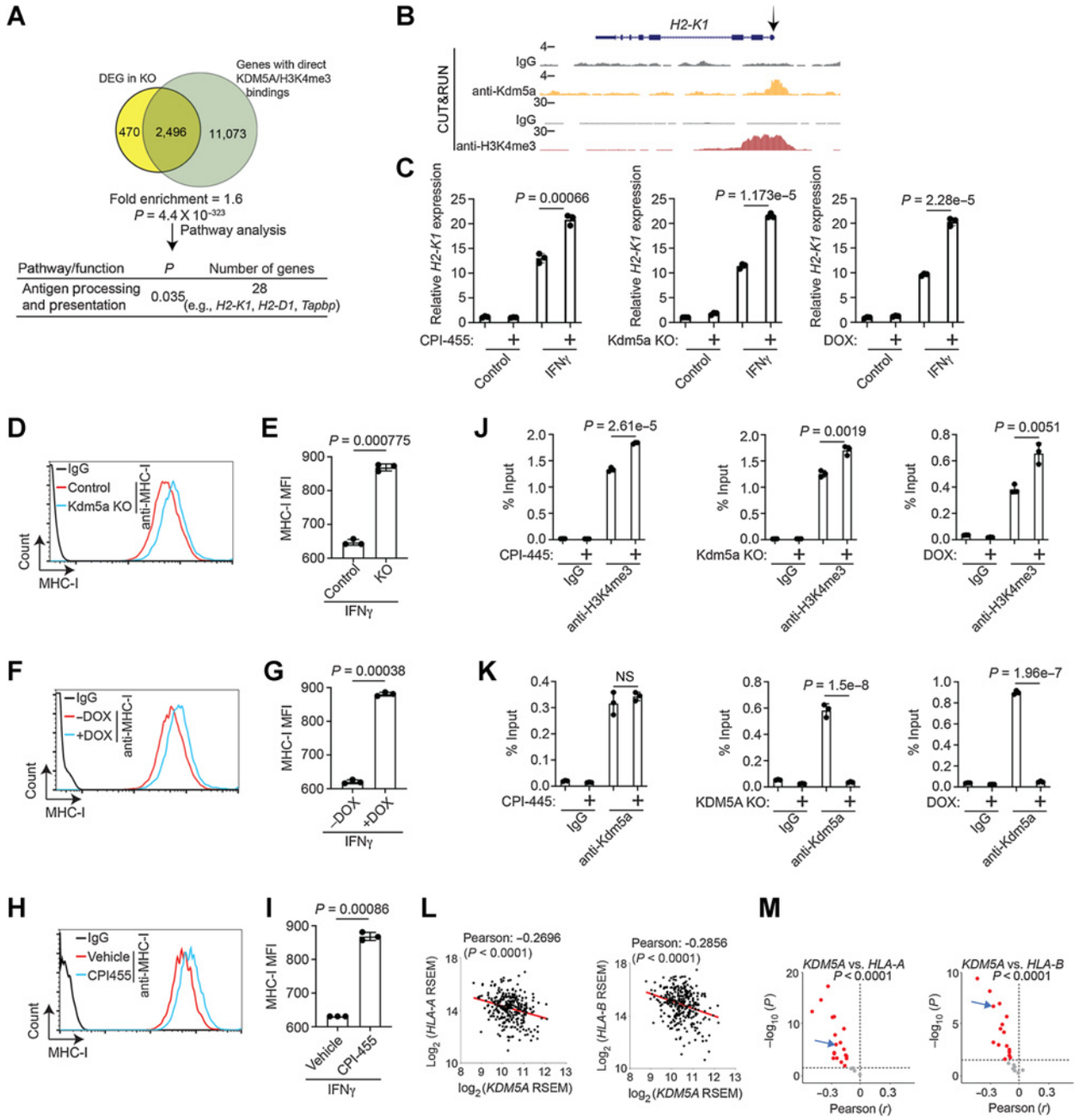

Figure 4.

KDM5A regulates antigen processing and presentation pathway. **A,** Experimental strategy used to identify Kdm5a direct target genes. GSEA pathway analysis revealed that the antigen processing and presentation pathway was enriched for the identified Kdm5a direct target genes (including *H2-K1*, *H2-D1*, and *Tapbp*). **B,** CUT&RUN tracks of the newly identified Kdm5a target gene *H2-K1* for Kdm5a and H3K4me3 in ID8 cells. **C,** Expression of *H2-K1* in doxycycline-inducible shKdm5a ID8 cells, Kdm5a inhibitor CPI-455, or Kdm5a-KO cells with or without IFNγ stimulation determined by qRT-PCR. **D,** Cell surface expression of H2-K1 in control and Kdm5a-KO ID8 cells with or without IFNγ stimulation was determined by FACS analysis. **E,** Quantification of (**D**). **F,** Cell surface expression of H2-K1 in control and doxycycline-inducible Kdm5a-knockdown ID8 cells with or without IFNγ stimulation was determined by FACS analysis. **G,** Quantification of (**F**). **H,** Cell surface expression of H2-K1 in D8 cells treated with vehicle or CPI-455 with or without IFNγ stimulation was determined by FACS analysis. **I,** Quantification of (**H**). An isotype-matched IgG was used as a negative control for all the FACS analysis. ID8 cells treated with or without CPI455, Kdm5a KO or inducible Kdm5a knockdown were treated with IFNγ and then subjected to ChIP analysis using anti-H3K4me3 (**J**) or anti-KDM5A (**K**) antibodies. **L,** Correlation between *KDM5*A and *HLA-A* or *HLA-B* expression based on RNA-seq analysis in the TCGA HGSOC dataset. **M,** Significant correlation between *KDM5A* and *HLA-A* or *HLA-B* expression based on RNA-seq analysis from 24 TCGA cancer types with at least 100 patients. The arrows point to HGSOCs. Data represent mean ±SEM of three biological repeats; *P* was calculated by using a two-tailed Student *t* test except in (**L**) by using Pearson *r* analysis test and in (**M**) by using Fisher exact test.

H3K4me3 (**Fig. 4A**). Pathway analysis revealed that one of the top functional pathways enriched in *Kdm5a*-KO cells was the antigen processing and presentation pathway ($P = 0.035$; **Fig. 4A**; Supplementary Fig. S4B and S4C). The three top ranked genes (namely *H2-K1*, *H2-D1*, and *Tapbp1*) in the list all encode key proteins involved in MHC class I–mediated antigen-presentation (**Fig. 4A**; Supplementary Fig. S4D). Inhibition of the MHC class I antigen-presentation pathway has been shown to be one of the major mechanisms underlying poor immune cell infiltration of tumors (8). One of the roles of the MHC class I complex is to present cancer cell antigens to cytotoxic $CD8^+$ T cells. H2-K1 (orthologous to the human HLA-A) is a component of the MHC class I complex and its decreased expression on the surface of cancer cells results in reduced immune infiltration of tumors and impaired antitumor immune responses (12–14). Our CUT&RUN analysis revealed that Kdm5a and H3K4me3 were enriched at the promoter of the mouse *H2-K1* gene (**Fig. 4B**).

We first sought to validate upregulation of *H2-K1* expression by Kdm5a inhibition in response to IFNγ treatment, which is known to promote expression of MHC class I genes to regulate the antitumor immune response (51). Specifically, the upregulation of ID8 expression of the *H2-K1* gene in response to IFNγ was further upregulated by the KDM5A inhibitor CPI-455 treatment (**Fig. 4C**). Likewise, *Kdm5a* KO or doxycycline-inducible knockdown of Kdm5a also increased the expression of the *H2-K1* gene in response to IFNγ treatment (**Fig. 4C**). *Kdm5a* KO or knockdown increased MHC class I presence on the surface of ID8 and HGS2 cells in response to IFNγ stimulation (**Fig. 4D–G**; Supplementary Fig. S4E–S4G). Similarly, CPI-455 treatment increased MHC class I presence on cell surface in response to IFNγ treatment (**Fig. 4H** and **I**; Supplementary Fig. S4H and S4I). We next validated changes in the association of H3K4me3 with the *H2-K1* gene promoter upon Kdm5a inhibition (**Fig. 4J**), which inversely correlated with the changes in its association with Kdm5a (**Fig. 4K**). However, CPI-455 increased the association of H3K4me3, but not Kdm5a, with the *H2-K1* gene promoter (**Fig. 4J** and **K**), which is consistent with the notion that CPI-455 inhibits the enzymatic activity of KDM5A instead of its association with its target genes.

To further support our observation that KDM5A regulates the expression of the MHC class I complex we analyzed the TCGA HGSOC dataset. We found that in HGSOC, *KDM5A* expression negatively correlated with two major subunits of human MHC class I complex, *HLA-A* and *HLA-B* (**Fig. 4L**). A negative correlation between *KDM5A* expression and *HLA-A* or *HLA-B* expression also was observed in a statistically significant majority of the cancer types in the 24 TCGA datasets with more than 100 patients (**Fig. 4M**; Supplementary Table S4). In addition, *HLA-A* and *HLA-B* expression highly correlated with expression of *CD8A* as well as *GZMB* in the TCGA HGSOC dataset (Supplementary Fig. S4J and S4K). Together, our data supports the notion that KDM5A exhibits oncogenic function through downregulation of antigen processing and presentation machinery such as the MHC class I complex.

Discussion

Our data demonstrate that KDM5A regulates antitumor immune responses. Mechanistically, we found that KDM5A suppresses the expression of genes involved in the antigen processing and presentation pathway. Specifically, we show that KDM5A regulates expression of MHC class I pathway genes such as *H2-K1*, and this correlates with a decreased presence of MHC class I on the surface of cancer cells. The MHC class I complex is responsible for tumor antigen-presentation to cytotoxic $CD8^+$ T cells and low levels of MHC class I expression is associated with reduced immune infiltration in several types of cancer (12–14). However, we cannot rule out the possibility that other mechanisms such as upregulation of chemokines induced by KDM5A inhibition may also contribute to the observed changes in infiltration of $CD8^+$ T cells. We found that expression of antigen-presentation genes repressed by Kdm5a could be restored by a small molecule inhibitor, CPI-455. However, a recent study showed that in a melanoma mouse model, the reduced expression of MHC class I expression does not affect $CD8^+$ T-cell infiltration (52). This suggests that the role of MHC class I in regulating $CD8^+$ T-cell infiltration may be cancer type– and/or context-dependent. Regardless, our *in vivo* studies demonstrated that Kdm5a inhibition resulted in increased $CD8^+$ T-cell infiltration, decreased ascites formations, and improved survival of tumor-bearing mice.

KDM5A plays a context-dependent role in cancer. Despite the evidence supporting an overall oncogenic role for KDM5A in several types of cancer (15, 16), we and other groups have not observed decreased cell viability upon KDM5A inhibition *in vitro* (27). Likewise, we show here that Kdm5a inhibition failed to significantly suppress tumor growth in immunocompromised mouse models. However, multiple studies have demonstrated that KDM5A may promote cancer *in vivo* by regulating cell cycle, invasion, EMT and chemoresistance (15, 16, 20–23). Regardless, our results support that KDM5A inhibition could potentially be a viable cancer therapeutic strategy through boosting antitumor immunity.

Several studies have demonstrated the role of KDM5A and other KDM5 family members in the regulation of antitumor immune responses. For example, increased expression of KDM5A improves the response to immune checkpoint blockade in a melanoma mouse model, and this was attributed to an overall higher recruitment of $CD8^+$ T cells due to changes in the myeloid compartment (50). However, our data showed that KDM5A inhibition promotes $CD8^+$ T cells and we did not observe a significant change in myeloid cells, indicating that KDM5A's role in regulating the tumor immune microenvironment may be cancer-type– and/or context-dependent. Other members of the KDM5 family such as KDM5B, but not KDM5A, have been shown to repress the immune response via suppression of the STING pathway (53). KDM5B also promotes immune evasion by epigenetic silencing of transposable elements (54). Together with the present study, these findings support the notion that KDM5 family proteins play a role in regulating antitumor immune responses.

Immune surveillance evasion is a major obstacle to overcome in developing effective EOC immunotherapy and our present study suggests KDM5A may play a role in this process. Therefore, the results presented here may serve as a scientific rationale for targeting KDM5A overexpressed EOCs, which represents approximately 26% of HGSOCs (55). Several KDM5A or pan-KDM5 inhibitors have been developed and are under various stages of preclinical evaluations (27). In addition to HGSOC, our results show that *KDM5A* expression negatively correlates with the expression of antigen-presentation genes in the majority of cancer types. Thus, it is possible that the findings presented here may be broadly applicable to other cancer types and it will be interesting to investigate the role of KDM5A in controlling antigen-presentation and infiltration of $CD8^+$ T cells in other cancer types. In summary, our results demonstrate that targeting KDM5A demethylase activity represents a viable therapeutic strategy to boost antitumor immunity.

Authors' Disclosures

R. Drapkin reports personal fees and nonfinancial support from Repare Therapeutics; and personal fees from VOC Health outside the submitted work. B.G. Bitler reports grants from the U.S. Department of Defense and NIH/NCI during the conduct of the study; other support from Onconic Therapeutics outside the submitted work. S. Karakashev reports grants from NIH/NCI during the conduct of the study. No disclosures were reported by the other authors.

Authors' Contributions

H. Liu: Data curation, formal analysis, validation, investigation, visualization, methodology, writing–original draft, writing–review and editing. **J. Lin:** Data curation, formal analysis, validation, investigation, visualization, methodology. **W. Zhou:** Data curation, investigation. **R. Moses:** Data curation, formal analysis, validation, investigation, visualization. **Z. Dai:** Data curation, investigation. **A.V. Kossenkov:** Formal analysis, methodology, writing–original draft. **R. Drapkin:** Resources. **B.G. Bitler:** Resources. **S. Karakashev:** Conceptualization, data curation, formal analysis, supervision, funding acquisition, validation, investigation, visualization, methodology, writing–original draft, writing–review and editing. **R. Zhang:** Conceptualization, supervision, funding acquisition, writing–original draft, project administration, writing-review and editing.

Acknowledgments

This work was supported by NIH grants (grant nos. R01CA202919, R01CA239128, and P50CA228991 to R. Zhang; grant no. K99CA241395 to S. Karakashev), the U.S. Department of Defense (OC180109 and OC190181 to R. Zhang). Support of Core Facilities was provided by Cancer Centre Support Grant (CCSG; grant no. CA010815 to The Wistar Institute).

The costs of publication of this article were defrayed in part by the payment of page charges. This article must therefore be hereby marked *advertisement* in accordance with 18 U.S.C. Section 1734 solely to indicate this fact.

Received February 2, 2022; revised March 31, 2022; accepted May 26, 2022; published first June 21, 2022.

References

1. Fridman WH, Zitvogel L, Sautes-Fridman C, Kroemer G. The immune contexture in cancer prognosis and treatment. Nat Rev Clin Oncol 2017;14:717–34.
2. Fridman WH, Galon J, Dieu-Nosjean MC, Cremer I, Fisson S, Damotte D, et al. Immune infiltration in human cancer: prognostic significance and disease control. Curr Top Microbiol Immunol 2011;344:1–24.
3. Bruni D, Angell HK, Galon J. The immune contexture and Immunoscore in cancer prognosis and therapeutic efficacy. Nat Rev Cancer 2020;20:662–80.
4. Topper MJ, Vaz M, Chiappinelli KB, DeStefano Shields CE, Niknafs N, Yen RC, et al. Epigenetic therapy ties MYC depletion to reversing immune evasion and treating lung cancer. Cell 2017;171:1284–300.
5. Dunn J, Rao S. Epigenetics and immunotherapy: The current state of play. Mol Immunol 2017;87:227–39.
6. Cao J, Yan Q. Cancer epigenetics, tumor immunity, and immunotherapy. Trends Cancer 2020;6:580–92.
7. Hogg SJ, Beavis PA, Dawson MA, Johnstone RW. Targeting the epigenetic regulation of antitumour immunity. Nat Rev Drug Discov 2020;19:776–800.
8. Jhunjhunwala S, Hammer C, Delamarre L. Antigen presentation in cancer: insights into tumour immunogenicity and immune evasion. Nat Rev Cancer 2021;21:298–312.
9. Garrido F, Algarra I, Garcia-Lora AM. The escape of cancer from T lymphocytes: immunoselection of MHC class I loss variants harboring structural-irreversible "hard" lesions. Cancer Immunol Immunother 2010;59:1601–6.
10. Wieczorek M, Abualrous ET, Sticht J, Alvaro-Benito M, Stolzenberg S, Noe F, et al. Major histocompatibility complex (MHC) class I and MHC class II proteins: Conformational plasticity in antigen presentation. Front Immunol 2017;8:292.
11. Vesely MD, Kershaw MH, Schreiber RD, Smyth MJ. Natural innate and adaptive immunity to cancer. Annu Rev Immunol 2011;29:235–71.
12. Dhatchinamoorthy K, Colbert JD, Rock KL. Cancer immune evasion through loss of MHC class I antigen presentation. Front Immunol 2021;12:636568.
13. Dersh D, Holly J, Yewdell JW. A few good peptides: MHC class I-based cancer immunosurveillance and immunoevasion. Nat Rev Immunol 2021;21:116–28.
14. Burr ML, Sparbier CE, Chan KL, Chan YC, Kersbergen A, Lam EYN, et al. An evolutionarily conserved function of polycomb silences the MHC class I antigen presentation pathway and enables immune evasion in cancer. Cancer Cell 2019;36:385–401.
15. Yang GJ, Zhu MH, Lu XJ, Liu YJ, Lu JF, Leung CH, et al. The emerging role of KDM5A in human cancer. J Hematol Oncol 2021;14:30.
16. Plch J, Hrabeta J, Eckschlager T. KDM5 demethylases and their role in cancer cell chemoresistance. Int J Cancer 2019;144:221–31.
17. Christensen J, Agger K, Cloos PA, Pasini D, Rose S, Sennels L, et al. RBP2 belongs to a family of demethylases, specific for tri-and dimethylated lysine 4 on histone 3. Cell 2007;128:1063–76.
18. Shilatifard A. Molecular implementation and physiological roles for histone H3 lysine 4 (H3K4) methylation. Curr Opin Cell Biol 2008;20:341–8.
19. Howe FS, Fischl H, Murray SC, Mellor J. Is H3K4me3 instructive for transcription activation? Bioessays 2017;39:1–12.
20. Beshiri ML, Holmes KB, Richter WF, Hess S, Islam AB, Yan Q, et al. Coordinated repression of cell cycle genes by KDM5A and E2F4 during differentiation. Proc Natl Acad Sci U S A 2012;109:18499–504.
21. Dai B, Huang H, Guan F, Zhu G, Xiao Z, Mao B, et al. Histone demethylase KDM5A inhibits glioma cells migration and invasion by down regulating ZEB1. Biomed Pharmacother 2018;99:72–80.
22. Feng T, Wang Y, Lang Y, Zhang Y. KDM5A promotes proliferation and EMT in ovarian cancer and closely correlates with PTX resistance. Mol Med Rep 2017;16:3573–80.
23. Banelli B, Carra E, Barbieri F, Wurth R, Parodi F, Pattarozzi A, et al. The histone demethylase KDM5A is a key factor for the resistance to temozolomide in glioblastoma. Cell Cycle 2015;14:3418–29.
24. Nie Z, Shi L, Lai C, O'Connell SM, Xu J, Stansfield RK, et al. Structure-based design and discovery of potent and selective KDM5 inhibitors. Bioorg Med Chem Lett 2018;28:1490–4.
25. Horton JR, Liu X, Gale M, Wu L, Shanks JR, Zhang X, et al. Structural basis for KDM5A histone lysine demethylase inhibition by diverse compounds. Cell Chem Biol 2016;23:769–81.
26. Gehling VS, Bellon SF, Harmange JC, LeBlanc Y, Poy F, Odate S, et al. Identification of potent, selective KDM5 inhibitors. Bioorg Med Chem Lett 2016;26:4350–4.
27. Yang GJ, Wu J, Miao L, Zhu MH, Zhou QJ, Lu XJ, et al. Pharmacological inhibition of KDM5A for cancer treatment. Eur J Med Chem 2021;226:113855.
28. Lin J, Liu H, Fukumoto T, Zundell J, Yan Q, Tang CA, et al. Targeting the IRE1alpha/XBP1s pathway suppresses CARM1-expressing ovarian cancer. Nat Commun 2021;12:5321.
29. Jordan KR, Sikora MJ, Slansky JE, Minic A, Richer JK, Moroney MR, et al. The capacity of the ovarian cancer tumor microenvironment to integrate inflammation signaling conveys a shorter disease-free interval. Clin Cancer Res 2020;26:6362–73.
30. Watson ZL, Yamamoto TM, McMellen A, Kim H, Hughes CJ, Wheeler LJ, et al. Histone methyltransferases EHMT1 and EHMT2 (GLP/G9A) maintain PARP inhibitor resistance in high-grade serous ovarian carcinoma. Clin Epigenetics 2019;11:165.
31. Chen B, Khodadoust MS, Liu CL, Newman AM, Alizadeh AA. Profiling tumor infiltrating immune cells with CIBERSORT. Methods Mol Biol 2018;1711:243–59.
32. Langmead B, Salzberg SL. Fast gapped-read alignment with Bowtie 2. Nat Methods 2012;9:357–9.
33. Li B, Dewey CN. RSEM: accurate transcript quantification from RNA-Seq data with or without a reference genome. BMC Bioinf 2011;12:323.
34. Langmead B, Trapnell C, Pop M, Salzberg SL. Ultrafast and memory-efficient alignment of short DNA sequences to the human genome. Genome Biol 2009;10:R25.
35. Heinz S, Benner C, Spann N, Bertolino E, Lin YC, Laslo P, et al. Simple combinations of lineage-determining transcription factors prime cis-regulatory elements required for macrophage and B cell identities. Mol Cell 2010;38:576–89.

36. Subramanian A, Tamayo P, Mootha VK, Mukherjee S, Ebert BL, Gillette MA, et al. Gene set enrichment analysis: a knowledge-based approach for interpreting genome-wide expression profiles. Proc Natl Acad Sci U S A 2005;102:15545–50.
37. Patch AM, Christie EL, Etemadmoghadam D, Garsed DW, George J, Fereday S, et al. Whole-genome characterization of chemoresistant ovarian cancer. Nature 2015;521:489–94.
38. Mok SC, Bonome T, Vathipadiekal V, Bell A, Johnson ME, Wong KK, et al. A gene signature predictive for outcome in advanced ovarian cancer identifies a survival factor: microfibril-associated glycoprotein 2. Cancer Cell 2009;16:521–32.
39. Tone AA, Begley H, Sharma M, Murphy J, Rosen B, Brown TJ, et al. Gene expression profiles of luteal phase fallopian tube epithelium from BRCA mutation carriers resemble high-grade serous carcinoma. Clin Cancer Res 2008;14:4067–78.
40. Augello G, Emma MR, Cusimano A, Azzolina A, Montalto G, McCubrey JA, et al. The role of GSK-3 in cancer immunotherapy: GSK-3 inhibitors as a new frontier in cancer treatment. Cells 2020;9:1427.
41. Zhong L, Yang Z, Lei D, Li L, Song S, Cao D, et al. Bromodomain 4 is a potent prognostic marker associated with immune cell infiltration in breast cancer. Basic Clin Pharmacol Toxicol 2021;128:169–82.
42. Shao S, Cao H, Wang Z, Zhou D, Wu C, Wang S, et al. CHD4/NuRD complex regulates complement gene expression and correlates with CD8 T cell infiltration in human hepatocellular carcinoma. Clin Epigenetics 2020;12:31.
43. Hwang WT, Adams SF, Tahirovic E, Hagemann IS, Coukos G. Prognostic significance of tumor-infiltrating T cells in ovarian cancer: a meta-analysis. Gynecol Oncol 2012;124:192–8.
44. Bachmayr-Heyda A, Aust S, Heinze G, Polterauer S, Grimm C, Braicu EI, et al. Prognostic impact of tumor infiltrating CD8+ T cells in association with cell proliferation in ovarian cancer patients–a study of the OVCAD consortium. BMC Cancer 2013;13:422.
45. Ovarian Tumor Tissue Analysis C, Goode EL, Block MS, Kalli KR, Vierkant RA, Chen W, et al. Dose-response association of CD8+ tumor-infiltrating lymphocytes and survival time in high-grade serous ovarian cancer. JAMA Oncol 2017;3:e173290.
46. Vinogradova M, Gehling VS, Gustafson A, Arora S, Tindell CA, Wilson C, et al. An inhibitor of KDM5 demethylases reduces survival of drug-tolerant cancer cells. Nat Chem Biol 2016;12:531–8.
47. Leadem BR, Kagiampakis I, Wilson C, Cheung TK, Arnott D, Trojer P, et al. A KDM5 inhibitor increases global H3K4 trimethylation occupancy and enhances the biological efficacy of 5-Aza-2'-deoxycytidine. Cancer Res 2018;78:1127–39.
48. Du W, Zhang L, Brett-Morris A, Aguila B, Kerner J, Hoppel CL, et al. HIF drives lipid deposition and cancer in ccRCC via repression of fatty acid metabolism. Nat Commun 2017;8:1769.
49. Kipps E, Tan DS, Kaye SB. Meeting the challenge of ascites in ovarian cancer: new avenues for therapy and research. Nat Rev Cancer 2013;13:273–82.
50. Wang L, Gao Y, Zhang G, Li D, Wang Z, Zhang J, et al. Enhancing KDM5A and TLR activity improves the response to immune checkpoint blockade. Sci Transl Med 2020;12:eaax2282.
51. Castro F, Cardoso AP, Goncalves RM, Serre K, Oliveira MJ. Interferon-gamma at the crossroads of tumor immune surveillance or evasion. Front Immunol 2018;9:847.
52. Moustaki A, Crawford JC, Alli S, Fan Y, Boi S, Zamora AE, et al. Antigen cross-presentation in young tumor-bearing hosts promotes CD8(+) T cell terminal differentiation. Sci Immunol 2022;7:eabf6136.
53. Wu L, Cao J, Cai WL, Lang SM, Horton JR, Jansen DJ, et al. KDM5 histone demethylases repress immune response via suppression of STING. PLoS Biol 2018;16:e2006134.
54. Zhang SM, Cai WL, Liu X, Thakral D, Luo J, Chan LH, et al. KDM5B promotes immune evasion by recruiting SETDB1 to silence retroelements. Nature 2021;598:682–7.
55. Cancer Genome Atlas Research Network. Integrated genomic analyses of ovarian carcinoma. Nature 2011;474:609–15.